LIMNOLOGY
and
OCEANOGRAPHY

ASLO

Limnol. Oceanogr. 62, 2017, 736–753

doi: 10.1002/lno.10456

Spectral wave dissipation by submerged aquatic vegetation in a back-barrier estuary

Daniel J. Nowacki,* Alexis Beudin, Neil K. Ganju
U.S. Geological Survey, Woods Hole Coastal and Marine Science Center, Woods Hole, Massachusetts

Abstract

Submerged aquatic vegetation is generally thought to attenuate waves, but this interaction remains poorly characterized in shallow-water field settings with locally generated wind waves. Better quantification of wave–vegetation interaction can provide insight to morphodynamic changes in a variety of environments and also is relevant to the planning of nature-based coastal protection measures. Toward that end, an instrumented transect was deployed across a *Zostera marina* (common eelgrass) meadow in Chincoteague Bay, Maryland/Virginia, U.S.A., to characterize wind-wave transformation within the vegetated region. Field observations revealed wave-height reduction, wave-period transformation, and wave-energy dissipation with distance into the meadow, and the data informed and calibrated a spectral wave model of the study area. The field observations and model results agreed well when local wind forcing and vegetation-induced drag were included in the model, either explicitly as rigid vegetation elements or implicitly as large bed-roughness values. Mean modeled parameters were similar for both the explicit and implicit approaches, but the spectral performance of the explicit approach was poor compared to the implicit approach. The explicit approach over-predicted low-frequency energy within the meadow because the vegetation scheme determines dissipation using mean wavenumber and frequency, in contrast to the bed-friction formulations, which dissipate energy in a variable fashion across frequency bands. Regardless of the vegetation scheme used, vegetation was the most important component of wave dissipation within much of the study area. These results help to quantify the influence of submerged aquatic vegetation on wave dynamics in future model parameterizations, field efforts, and coastal-protection measures.

Submerged aquatic vegetation (SAV) alters the hydrodynamic and sedimentary regimes of riverine, estuarine, and coastal environments. Prior work illustrates the ability of SAV to modify unidirectional turbulent flows (reviewed in Nepf 2012), wave height (Mendez and Losada 2004; Paul and Amos 2011; Infantes et al. 2012), wave-orbital motions (Bradley and Houser 2009; Hansen and Reidenbach 2012), and wave-generated currents (Luhar et al. 2010) in model, laboratory, and field settings. Suspended-sediment concentration (SSC) near SAV may increase in sparse vegetation canopies, because of increased turbulence from stem wakes, or decrease in dense vegetation because of turbulence damping within the canopy (Nepf 2012). The interaction of waves and SAV may modify the grain-size characteristics of the seabed (van Katwijk et al. 2010) and waves may also control the distribution of SAV in shallow-water environments (Stevens and Lacy 2012). These wave–SAV interactions are closely related to biophysical feedbacks involving light availability, SSC, seabed composition, and vegetation characteristics. For example, a feedback loop may develop wherein vegetation reduces wave stresses, which leads to decreased sediment resuspension and increased light availability, and a resultant increase in vegetation biomass (Hansen and Reidenbach 2012).

In the aforementioned studies, local (re-) generation of waves was not considered. However, in limited-fetch environments like back-barrier lagoons, local winds are critical to the wave field, the resulting bed stress, sediment transport, and ultimately the character of the local geomorphology. In addition to measuring bulk quantities like significant wave height, wave period, and wave dissipation in vegetated regions, a full quantification of the spectral wave field is crucial to understanding the wave dynamics and potential feedbacks between seagrass, sediment transport, and light availability.

Wave–vegetation interaction models generally characterize vegetation as rigid cylinders with a constant drag

*Correspondence: dnowacki@usgs.gov

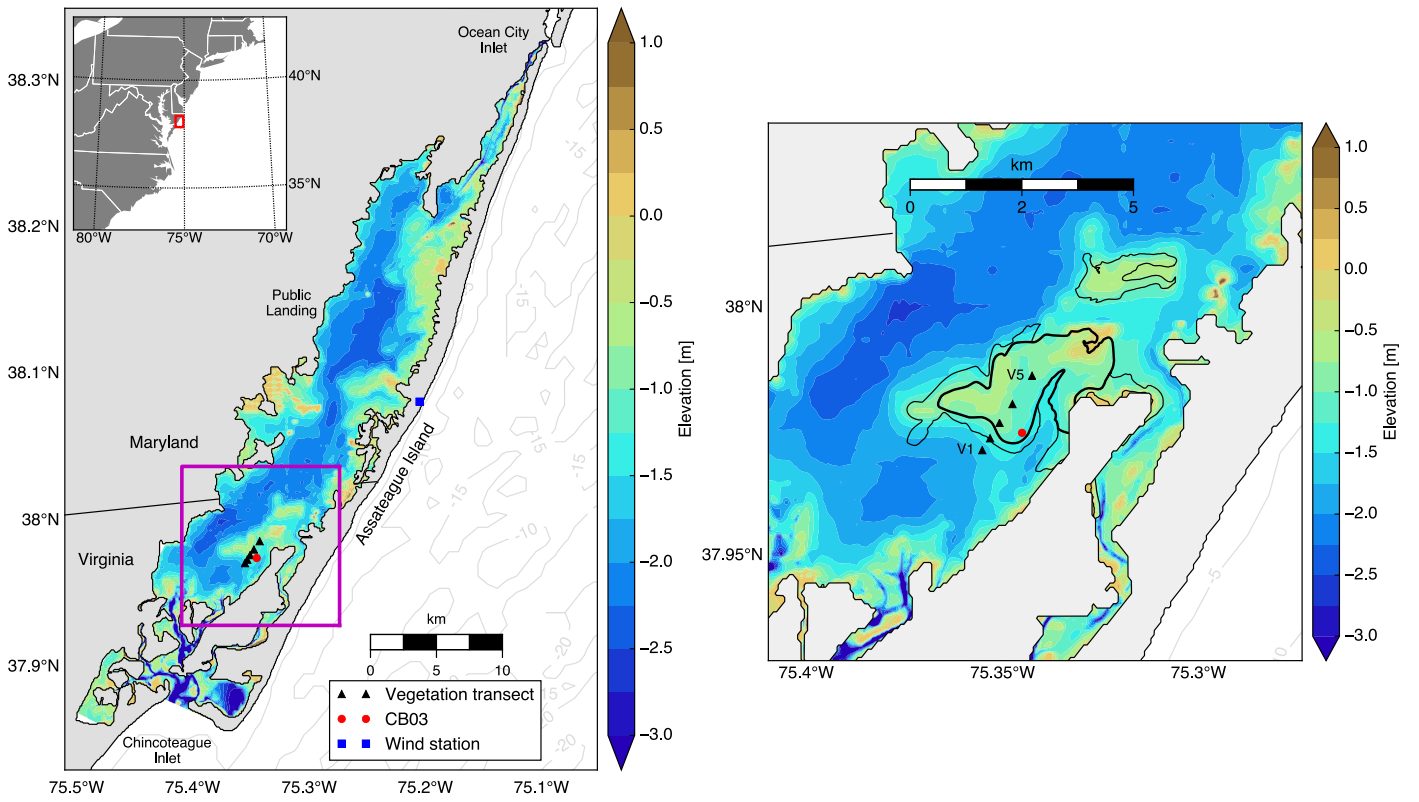

Fig. 1. Left: bathymetric map of Chincoteague Bay showing locations of the vegetation transect sites, long-term mooring CB03, and weather stations. Right: bathymetric map of vegetation transect area. Heavy black lines indicate areas of "dense" seagrass coverage during 2013; thinner lines indicate "moderate" seagrass coverage (Orth et al. 2014).

coefficient, following Dalrymple et al. (1984). In order to overcome the limitations inherent to this approach, and to represent some of the flexible character of natural vegetation, more recent studies have used variable drag coefficients (Kobayashi et al. 1993; Mendez and Losada 2004; Sánchez-González et al. 2011). Instead of implementing vegetation in an explicit manner, other studies have characterized vegetation implicitly by deriving an equivalent bottom roughness length that represents the dissipation from vegetation. These include Bradley and Houser (2009) who found an average roughness length of 0.16 m for *Thalassia testudinum*, Paul and Amos (2011) who derived a mean effective roughness value of 0.17 m for *Zostera noltii*, and Infantes et al. (2012) who computed a value of 0.40 m for *Posidonia oceanica*.

In general, wave-orbital velocities in vegetated regions tend to be reduced compared to waves above a denuded bed (Hansen and Reidenbach 2012). The vegetation may also act as a low-pass filter, with longer-period waves more easily able to penetrate the seagrass meadow (Bradley and Houser 2009; Hansen and Reidenbach 2012). The open questions regarding the interaction of locally generated waves and vegetation in shallow, open-water conditions motivates the work presented here. In this study, we describe the spectral characteristics and transformation of wind waves as observed in a shallow-water environment and test the efficacy of several modeling approaches in representing vegetation-induced wave dissipation in this setting.

Study area

Chincoteague Bay is a shallow microtidal back-barrier lagoon that straddles the Maryland–Virginia border on the east coast of the United States (Fig. 1). It receives little freshwater input and is connected to the Atlantic Ocean by Ocean City Inlet at its northern end and Chincoteague Inlet at the south. The long, narrow bay is oriented to the north-northeast/south-southwest and is approximately 55 km in length and 10 km in width, with a surface area of 380 km^2. The average depth of Chincoteague Bay is 1.4 m, and a deep (3 m) channel flanks the western side of the bay. The channel bed is predominantly mud, the source of which is primarily wetland erosion (Bartberger 1976). The shallower eastern side of the bay is sandier, having been formed by overwash from Assateague Island. Tides are greatest near Ocean City Inlet and Chincoteague Inlet, with mean tidal ranges of approximately 0.7 m. Mid bay, the tides are smaller, with a mean range of 0.16 m at Public Landing. These tidal ranges result in minimal tidal currents in the

majority of the bay. As a result, circulation in the bay is primarily wind driven.

In Chincoteague Bay, SAV coverage varies from year to year but generally is extensive; annual aerial surveys reveal areal extents between 25 km^2 and 60 km^2 for the period 2004–2014 (Orth et al. 2014). For 2014, the most recent year available, bay-wide SAV coverage was 35.2 km^2. The primary SAV species in Chincoteague Bay is *Zostera marina* (common eelgrass) (Orth et al. 2014), and the majority of the meadows are located on the sandier eastern flank of the bay.

As a back-barrier lagoon on the Atlantic coastal plain, Chincoteague Bay is subject to wind forcing in the form of episodic storms and daily sea breezes. Winds are bimodal, and include relatively strong northeasterly winds associated with passing storm systems as well as weaker, more frequent winds from the south–southwest. Wave conditions in the bay are controlled by and respond quickly to local wind forcing, with waves growing and decaying in concert with both daily breezes and larger events.

Methods

Field data collection

A linear transect of five instrumented platforms, V1–V5, was deployed across a *Z. marina* meadow in Chincoteague Bay (Fig. 1) during April–July 2015. This particular meadow, like most others in Chincoteague Bay, sits on a topographic high and was chosen because it is one of the largest persistent SAV features in the bay. The areal extent of the "dense" SAV coverage (Orth et al. 2014) in the meadow was approximately 5 km^2, and the instrumented transect was 2 km long. Bathymetry along the transect shoaled from the deepest site, V1, through site V2, to the shallowest site, V3, and then deepened slightly to sites V4 and V5 (Fig. 2). Although flat bathymetry would help isolate the effects of vegetation on waves, variable water depths are common in wave–vegetation field studies. Sites with bed slopes ranging from 1 : 100 to 1 : 1000 have been examined in the past (Bradley and Houser 2009; Paul and Amos 2011; Infantes et al. 2012); the maximum bed slope in this study is 1 : 1000. The transect orientation of 33°/213° was selected to be approximately aligned with the dominant wind directions of NE and SSW experienced in Chincoteague Bay.

At site V1, a 2 MHz Nortek Aquadopp Profiler collected mean flow profiles every 15 min and directional wave bursts every 30 min at a sampling frequency of 2 Hz. At sites V2–V5, RBR, Ltd. RBRvirtuoso wave/tide gauges collected wave bursts data every 30 min at a sampling frequency of 6 Hz. Average water depths at the sites were 0.7–1.7 m. Wind speed and direction data were obtained from a wind station approximately 17 km northeast of the transect on Assateague Island (Fig. 1).

In addition to considering the entire 2.5 month field deployment, we focus on two wind and wave events to isolate the influence of winds from different directions. The first, a 5 d moderate-wind event from the SW, occurred during late May 2015 (hereafter referred to as the northward wave event), and the second was a 3 d NNE event in early June 2015 (the southward wave event). Mean wind direction for each event was within 15° of the transect: during the northward event, the wind direction was 180°–220°, and during the southward event it was 25°–45°. The dominant wave direction at V1 was consistent with the wind direction measured at the Assateague wind station during both wind events.

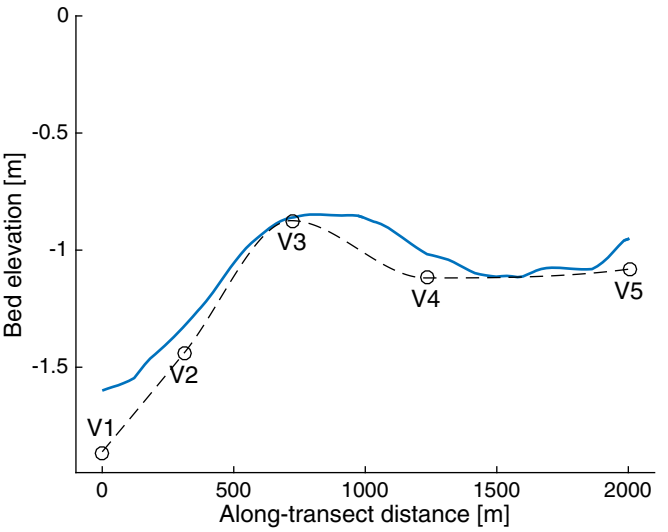

Fig. 2. Bathymetric profile along the vegetation transect (solid line), average water depths at V1–V5 from the April–July VT deployment (circles), and example interpolated bathymetry as used in the model (dashed line). The extracted bathymetric profile and measured water depths agree well. The maximum bed slope is approximately 1 : 1000.

Using triplicate 0.015 m^2 cores, SAV was characterized at two locations within the study area, one at V3 in April 2015 and the other at CB03, a nearby long-term mooring, in August 2014 and April 2015 (Table 1). Both locations were dominated by *Z. marina* (Fig. 3). At CB03, the average blade length was longer in August 2014 ($\sim$ 28 cm) than in April 2015 ($\sim$ 14 cm), while at V3 the average length was about 17 cm. Blade width was about 3 mm at all locations. Stem density was greater at V3, with nearly 2000 stems m^{-2}, than at CB03, which had about 900 stems m^{-2}. Because vegetation was quantified at only two locations, any fine-scale spatial variability of vegetation characteristics within the study area remains unknown.

In order to quantify the influence of bed roughness on waves, we used bed grain-size data obtained by the U.S. Geological Survey (Ellis et al. 2015). The seabed sediment texture (Folk 1954) was muddy sand in the vicinity of the study area with a median grain size of about 45 μm.

Table 1. Vegetation length (l_v in cm), width (b_v in mm), and density (N_v in stems m^{-2}) at sites CB03 and V3. Ranges indicate ± one standard deviation.

Site	l_v	b_v	N_v
August 2014			
CB03	27.7 ± 1.5	3.4 ± 0.0	907 ± 184
April 2015			
CB03	13.8 ± 3.3	3.1 ± 0.5	911 ± 385
V3	16.9 ± 1.3	2.9 ± 0.2	1955 ± 214

Field data analysis

Wave spectra and bulk wave characteristics were computed with DIWASP version 1.4 (Johnson 2011) using pressure and velocity data at V1 and pressure data at V2–V5. Significant wave height H_s was determined as

$$H_s = 4\sqrt{m_0},$$

where $m_0 = \int\int E(\sigma,\theta)d\sigma d\theta$ is the variance of the two-dimensional water-surface elevation spectrum $E(\sigma,\theta)$, which varies with frequency σ and direction θ. Mean wave period T_m was computed as

$$T_m = \frac{m_0}{m_1},$$

where $m_1 = \int\int \sigma E(\sigma,\theta)d\sigma d\theta$ is the first moment of $E(\sigma,\theta)$. Peak wave period T_p was determined as the wave period containing the greatest energy. Dominant wave direction D_p was determined as the compass direction containing the greatest energy integrated across all frequencies. This was a more stable parameter than the main direction of the peak period, which is the direction corresponding to the frequency band in the two-dimensional wave spectrum with the most energy. Wave spreading was computed from the directional wave spectra following Kuik et al. (1988).

The wave energy density flux $F = \frac{1}{2}\rho g a_j^2 c_{g,j}$ was computed for all frequencies at each site, where ρ is water density, g is acceleration due to gravity, a_j is the wave amplitude, and $c_{g,j}$ is the group velocity. The wave amplitude is defined as $a_j = H_j/2 = \sqrt{2E(\sigma,\theta)d\sigma d\theta}$.

Wave dissipation ϵ_j was computed for each frequency between adjacent sites:

$$\varepsilon_j = \frac{F_n - F_{n-1}}{\Delta r}, \quad (1)$$

where $\Delta r = \Delta x \cos\phi$ is the along-transect distance between sites. This value accounts for wave direction relative to the transect, wherein ϕ is the angle between the dominant wave direction and the transect orientation, and Δx is the distance between adjacent sites. Dissipation rates for each frequency j may be summed to compute the total wave energy dissipation:

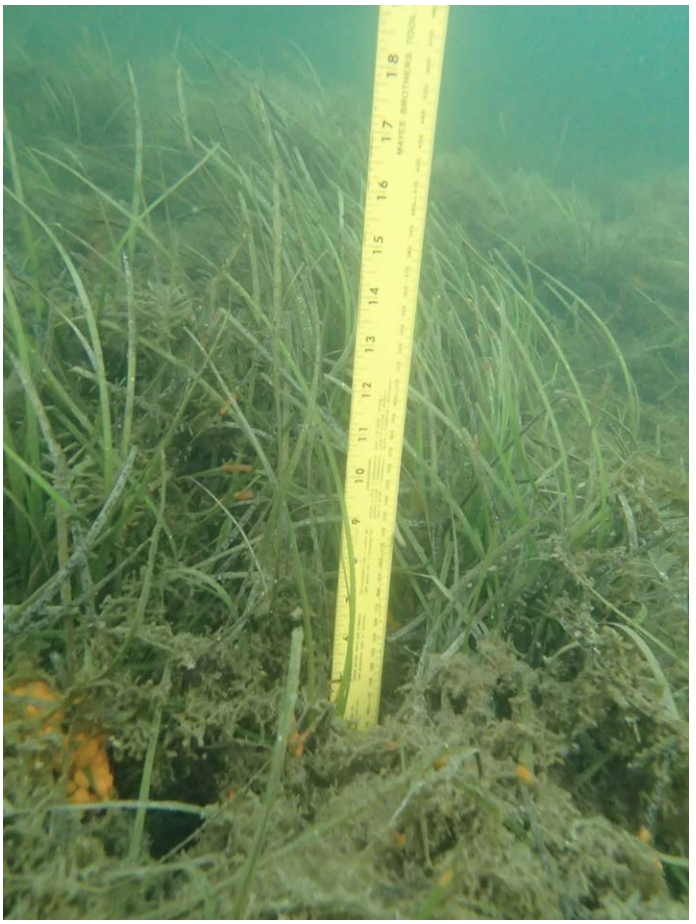

Fig. 3. Seagrass meadow in Chincoteague Bay. USGS photo.

$$\varepsilon = \sum \varepsilon_j. \quad (2)$$

One way to interpret wave dissipation rates is to normalize by the incident wave energy density flux:

$$\varepsilon_{j,\mathrm{norm}} = \frac{\varepsilon_j}{F_{n-1}}. \quad (3)$$

The normalized dissipation enables one to inspect relative dissipation rates across frequencies without the large signal imposed by the dependence of dissipation on wave height (Eq. 1).

Although the focus of this paper is dissipation from vegetation, other dissipation sources such as whitecapping, breaking, and bottom friction may be important, and are discussed in the next section.

In addition to being dissipated, waves may be reflected by steeply sloping bathymetry. The maximum slope along the vegetation transect was approximately 1 : 1000, indicating that wave reflection by topography was negligible (e.g., Booij 1983).

Numerical model

To augment the field observations, we implemented the spectral wave model SWAN (Booij et al. 1999) in the study area. SWAN version 41.01A was run in one-dimensional stationary mode to investigate the interplay among: the wave field as forced at the boundary; wave generation by locally forced winds; and wave dissipation by bed friction, vegetative drag, and other sources. Individual model runs were performed for each burst at the same 30 min time interval as the measured field data. The analyses below are based on 299 bursts with moderate to strong winds having a northward wind component from throughout the deployment. The model used a realistic but simplified bathymetry consisting of a cubic spline interpolation of measured water depths at the five stations for each burst (Fig. 2). The model was forced at V1 with the observed wave spectra, dominant direction, and spreading. For completeness, the effect of currents was included by applying the observed velocities at V1 across the model domain, but model results were not sensitive to the presence of currents. All model runs accounted for nonlinear energy transfer within the wave spectrum and dissipation from whitecapping, depth-induced breaking, and bottom friction, which are described in the following paragraphs.

Nonlinear wave-energy transfer may arise through triad and quadruplet wave–wave interaction, and these were accounted for in all runs. Triads shift energy from lower to higher frequencies in shallow water and also can generate higher wave harmonics. Quadruplets are generally important in deep water and can move energy both to higher and lower frequencies.

Dissipation from whitecapping can occur when waves become too steep as a result of bathymetric variability or from applied wind stress, and whitecapping was enabled in all model runs. The whitecapping formulations of Komen et al. (1984) and a modified form of Alves and Banner (2003) (SWAN Team 2015) were tested and produced similar results; those using the modified Alves and Banner (2003) approach are presented here.

In regions of rapid bathymetric change, depth-induced breaking could potentially be significant. To account for depth-induced wave breaking, we evaluate the breaking parameter γ:

$$\gamma = \frac{H_{\mathrm{rms}}}{h}, \tag{4}$$

where H_{rms} ($=H_s/\sqrt{2}$ for a Rayleigh distribution) is the root-mean-square wave height and h is the water depth. All γ values in the field data set were smaller than a conservative limit of $\gamma < 0.2$ (e.g., Paul and Amos 2011), suggesting that partially breaking waves were not present during the study. Nevertheless, depth-induced breaking was enabled in the model.

Bottom friction is implemented in SWAN using the general form (Booij et al. 1999; SWAN Team 2015)

$$S_{\mathrm{ds,b}} = -C_b \frac{\sigma^2}{g^2 \sinh^2 kh} E(\sigma,\theta), \tag{5}$$

where C_b is a bed friction coefficient and k is the wavenumber. The value and computation of C_b depends on the model used. In the case of Collins (1972), $C_b = C_f g u_{\mathrm{rms}}$, the dimensionless friction coefficient C_f is specified by the user, and the characteristic near-bed velcoity u_{rms} is computed at each location in the model. In Madsen et al. (1988), $C_b = f_w(g/\sqrt{2})u_{\mathrm{rms}}$. SWAN iteratively determines the dimensionless friction factor f_w from the near-bottom excursion amplitude A_b and the Nikuradse bottom roughness length k_s, as proposed by Jonsson (1966):

$$\frac{1}{4\sqrt{f_w}} + \log\left(\frac{1}{4\sqrt{f_w}}\right) = -0.08 + \log\left(\frac{A_b}{k_s}\right). \tag{6}$$

Equation 6 holds for $A_b/k_s > 1.57$; otherwise, $f_w = 0.3$. This sets an upper bound on the maximum value of k_s, effectively limiting the use of large k_s values to represent, in an implicit form, roughness elements like dense vegetation.

An alternative, direct method for determining f_w was proposed by Swart (1974), as modified by Nielsen (1992):

$$f_w = \exp\left[5.5\left(\frac{A_b}{k_s}\right)^{-0.2} - 6.3\right]. \tag{7}$$

Unlike Eq. 6, Eq. 7 imposes no upper limit on f_w. In both cases, a physically relevant quantity, the Nikuradse roughness length k_s, parameterizes the wave friction factor. This length generally is related to characteristics of the bed sediment; here we compute it as (Soulsby 1997):

$$k_s = 2.5 D_{50}. \tag{8}$$

The roughness length potentially could be extended to represent the drag from vegetation in an implicit manner if vegetation is much more important than bed friction in dissipating the waves, but the relation of k_s to the dimensions of the vegetation remains unclear.

Model runs

Six model runs were carried out to test the importance of energy input from wind and the efficacy of four different approaches in representing vegetation (Table 2). In Runs 1 and 2, the importance of wind on waves over an unvegetated seabed was tested. In Runs 3–6, four different formulations for representing vegetation under local wind forcing were considered: two which model vegetation explicitly as cylindrical elements and two which model vegetation implicitly with large bed roughness values.

Table 2. Description of model runs. The designation C72 refers to Collins (1972); M88 corresponds to Madsen et al. (1988). C_D: vegetation drag coefficient; KC: Keulegan–Carpenter number; k_s: Nikuradse bottom roughness length; C_f: Collins (1972) drag coefficient.

Run	Wind	Vegetation	Bed friction
1	No	No	M88, k_s=0.005 m
2	Yes	No	M88, k_s=0.005 m
3	Yes	Explicit, C_D=0.5	M88, k_s=0.005 m
4	Yes	Explicit, $C_D=22.9\mathrm{KC}^{-1.09}$	M88, k_s=0.005 m
5	Yes	Implicit in bed friction	C72, C_f=0.4
6	Yes	Implicit in bed friction	M88 k_s=0.03 m

To represent the effects of sediment-induced bed friction in the bed-only and explicit vegetation cases (Runs 1–4), the approach of Madsen et al. (1988) with k_s=0.005 m was used. This value corresponds to D_{50}=2000 μm (Eq. 8) and is 20 times greater than the equivalent length for the largest observed seabed grain size in the area. The use of such a large roughness length is intended to serve as an upper limit of reasonable grain (or bedform) roughnesses for comparison with larger roughness values meant to represent vegetation drag implicitly.

The importance of local wind in the model was tested in Runs 1 and 2 using winds measured at the Assateague wind station. Wind-induced wave growth was implemented in the model through both linear (Cavaleri and Rizzoli 1981) and exponential (Komen et al. 1984) growth terms using default values. Wind speed and direction used in the model were obtained from data collected at the Assateague wind station. SWAN expects wind measured at 10 m elevation, but the height of the Assateague station is 6.1 m; to account for this discrepancy, values measured at 6.1 m were estimated at 10 m following Hsu et al. (1994).

In Runs 3 and 4, vegetation was represented explicitly following the approach of Dalrymple et al. (1984). This method was developed originally for monochromatic waves and was extended to spectral wave fields by Mendez and Losada (2004). Vegetation elements are modeled as rigid cylinders and dissipation is from the drag force only. The vegetation dissipation source term is (Suzuki et al. 2012; SWAN Team 2015):

$$S_{\mathrm{veg}}=-\sqrt{\frac{2}{\pi}}g^2C_{\mathrm{D}}b_{\mathrm{v}}N_{\mathrm{v}}\left(\frac{\tilde{k}}{\tilde{\sigma}}\right)^3\frac{\sinh^3\tilde{k}\alpha h+3\sinh\tilde{k}\alpha h}{3\tilde{k}\cosh^3\tilde{k}h}\sqrt{E_{\mathrm{tot}}}\,E(\sigma,\theta), \tag{9}$$

where $\tilde{k}$ is the mean wavenumber (WAMDI Group 1988), $\tilde{\sigma}$ is the mean frequency, and $\alpha=h_v/h$ is the relative height of the vegetation. Vegetation parameters were selected using characteristic values from vegetation surveys at and near the vegetation transect (Table 1). For the model results presented here, vegetation height h_v=0.2 m, width b_v=0.003 m, and density N_v = 1800 stems m^{-2}. The vegetation drag coefficient C_D may be constant for all wave conditions or may vary with wave parameters, as described below.

An optimal value for the constant C_D case (Run 3) was obtained through sensitivity testing. Here, C_D was modified to obtain the best agreement in significant wave height, mean period, and net dissipation for 299 half-hourly bursts from throughout the 2.5 month deployment with moderate-to-strong northward winds.

Because of the significant assumptions inherent to the Dalrymple et al. (1984) approach, investigators have implemented variable C_D schemes as a way of including additional wave–vegetation processes, including plant swaying and the relationship between wave excursion and vegetation diameter or spacing. In addition to the constant C_D implementation, several formulations were tested in which C_D varied with the Keulegan–Carpenter number: $\mathrm{KC}=u_bT/b_v$, where u_b is the near-bed velocity and T is the wave period. Because the variable drag coefficient generally takes the form $C_D=\alpha\mathrm{KC}^{-\beta}$, C_D is large for small KC (i.e., high-frequency waves). The variable C_D approaches required modifications to the SWAN source code to compute C_D based on the Keulegan–Carpenter number. Model runs using variable C_D expressions from Mendez and Losada (2004), Bradley and Houser (2009), Sánchez-González et al. (2011), and Houser et al. (2015) were compared to the field data. The formulation of Sánchez-González et al. (2011), who carried out flume experiments on artificial *P. oceanica* (a Mediterranean seagrass) meadows, best reproduced the observed wave characteristics (H_s, T_m, and ϵ) during the late May northward wind event and was selected to compare against the constant C_D approach in Run 4. The variable C_D expression derived by Sánchez-González et al. (2011) is

$$C_{\mathrm{D}}=22.9\mathrm{KC}^{-1.09},\ 15\le\mathrm{KC}\le425. \tag{10}$$

In the implicit vegetation runs (Runs 5 and 6), bed friction and vegetation drag are combined into a single bed roughness parameter. We use in Run 5 the Collins (1972) formulation, the free parameter of which is a unitless drag coefficient (C_f) with no upper bound. For the 299 half-hourly bursts with northward waves considered here, a C_f value of 0.4 best matched the observations.

Run 6 represents vegetation implicitly using the formulation of Madsen et al. (1988). This approach is appealing because its free parameter is a roughness length, and it thereby maintains physical relevance. In its SWAN implementation, the Madsen et al. (1988) approach is not directly suitable for this purpose, because it solves for f_w following Jonsson (1966) (Eq. 6), which is valid only for $A_b/k_s > 1.57$; this sets an upper limit to k_s. In sensitivity testing, the use of roughness lengths greater than about 0.01 m produced A_b/k_s

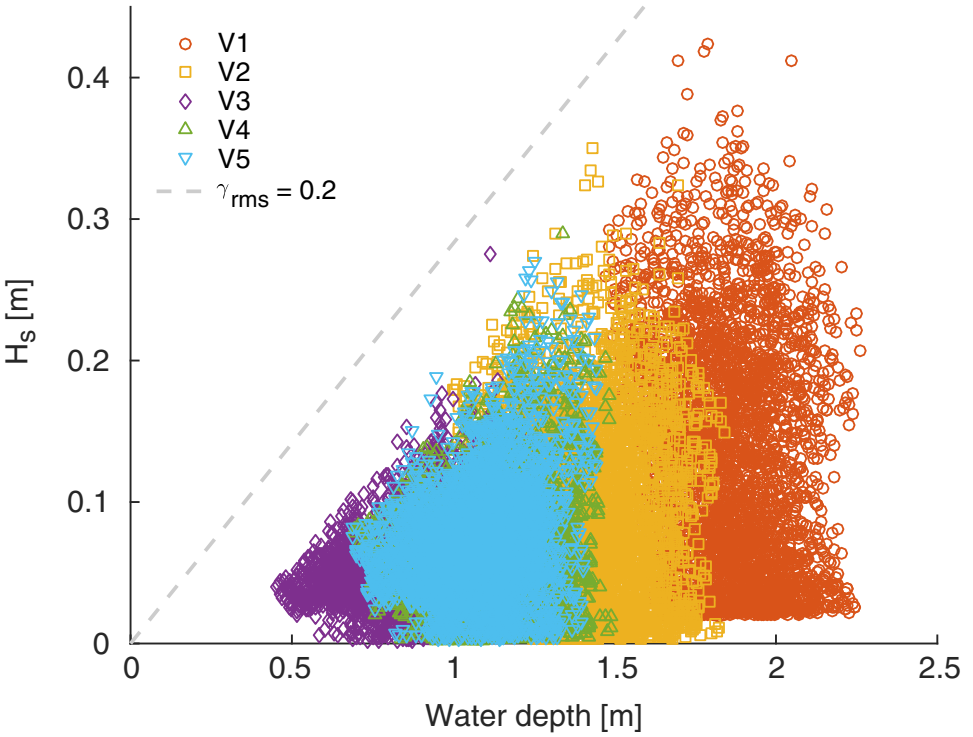

Fig. 4. Water depth vs. significant wave height for the five VT sites throughout the 2.5 month deployment. Maximum H_s increases with water depth, and maximum H_s values are less than a conservative breaking threshold of γ_{rms}=0.2.

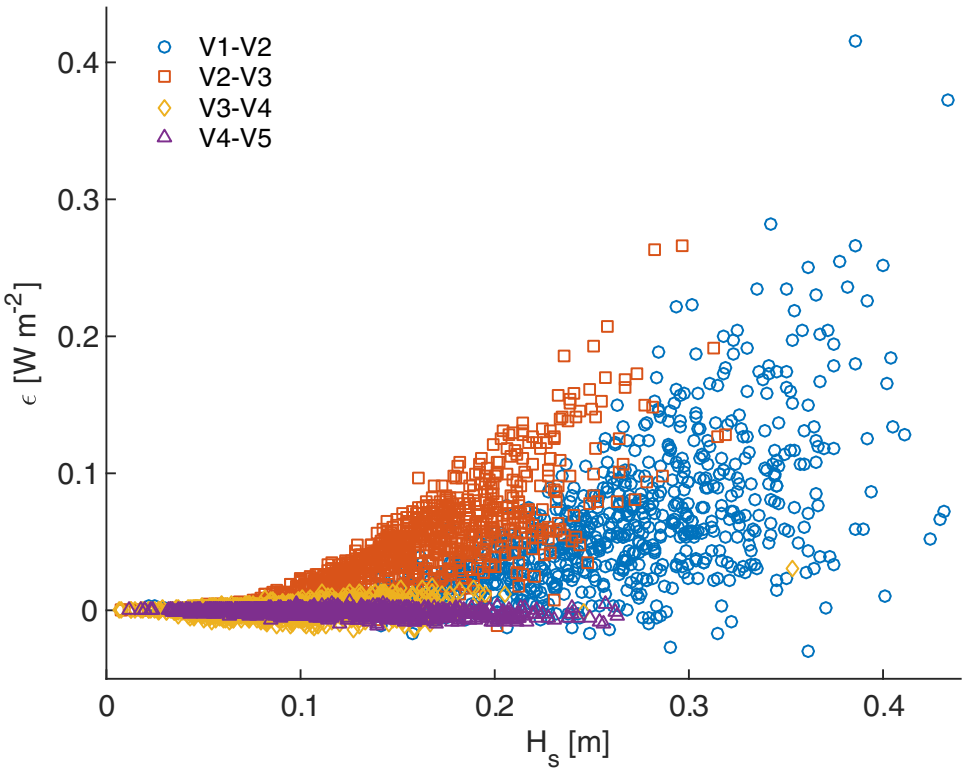

Fig. 5. Significant wave height vs. dissipation between pairs of sites. Northward wave conditions (D_p within ±20° of the transect orientation) from the full 2.5 month deployment are shown.

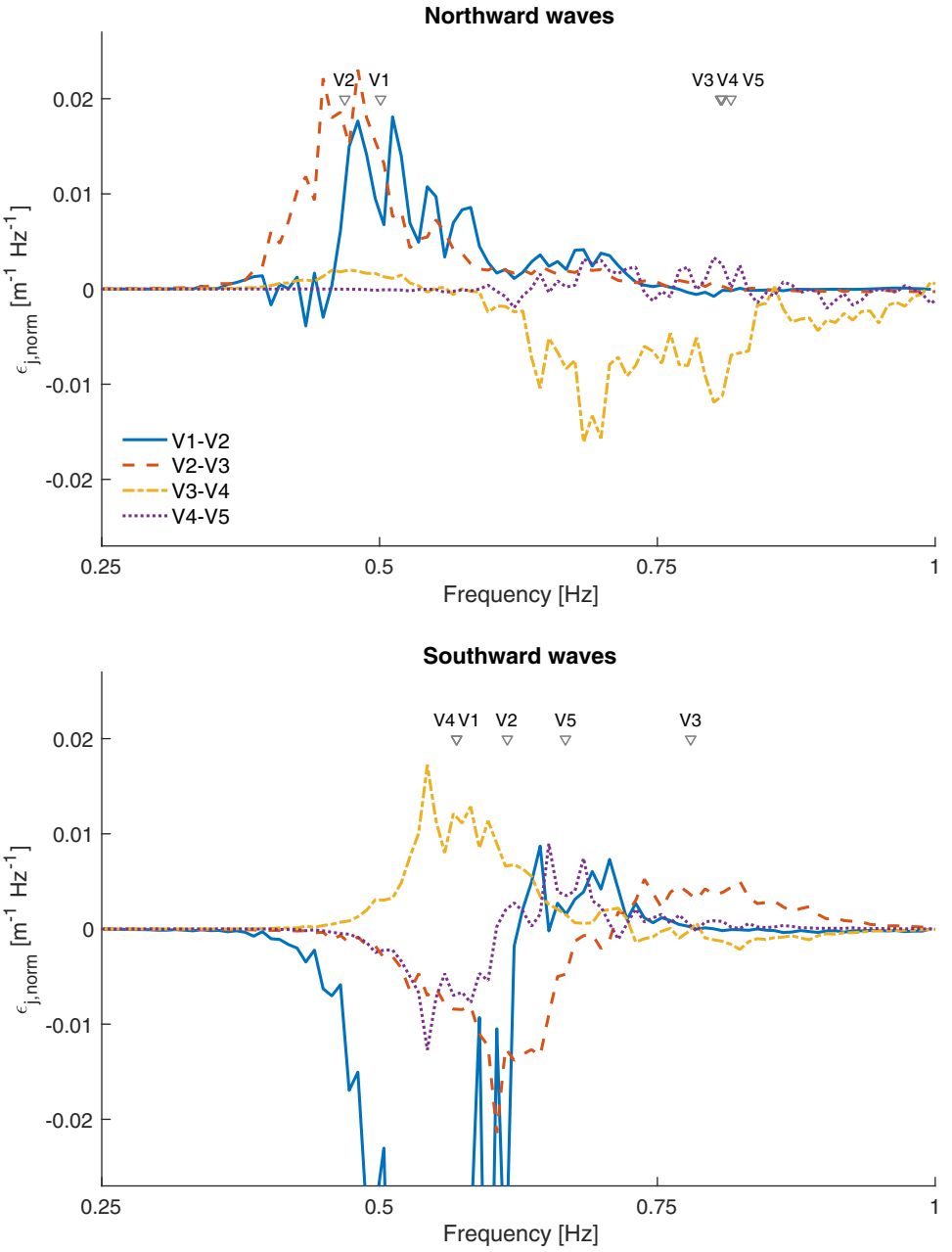

Fig. 6. Normalized dissipation as a function of frequency between each station pair during a period of (top) northward waves (20:30–21:30 on 27 May 2015) and (bottom) southward waves (13:30–15:00 on 04 June 2015). Peak frequencies ($f_p = 1/T_p$) at each station are indicated with triangles.

values less than 1.57 within the model domain, and the limiting f_w value of 0.3 was applied in those low A_b/k_s regions. Using this limiting roughness length (and corresponding f_w) resulted in poor agreement with the observational data, indicating that Jonsson (1966) cannot produce f_w values high enough for the drag present in the study area. We therefore implemented the direct-solution approach for determining f_w as proposed by Swart (1974) and modified by Nielsen (1992), which is valid for $A_b/k_s > 0.0369$, enabling selection of larger k_s values. This implementation involved modifying the SWAN source code to solve for f_w using Eq. 7, allowing us to represent more fully the drag imposed by the vegetation that otherwise would have been impossible with the original f_w equation.

Results

Field study

Wave characteristics

Wave heights ranged from essentially zero to a transect maximum H_s of about 0.4 m at V1. Throughout the deployment, H_s was largest at site V1, the deepest site, and smallest at site V3, the shallowest (Fig. 4). Mean H_s at V1 was 0.13 ± 0.09 m and 0.06 ± 0.03 m at V3, where ranges indicate the standard deviation of wave heights throughout the deployment. Waves generally decreased in height from V1 through V2–V3, grew slightly between V3 and V4, and lessened between V4 and V5. Maximum wave heights at and among stations scaled with water depth, as the maximum allowable wave height increased in deeper water in this depth-limited wave environment. Maximum γ values (Eq. 4) were always less than 0.2. In the surf zone on a sandy beach, only a small percentage of waves were observed to break for values of $\gamma \approx 0.2$ (Thornton and Guza 1983). That the observations were always less than this value suggests that, even though the waves were depth limited, depth-induced breaking was not significant along the vegetation transect. The longest wave periods were present at V1 (mean $T_m = 1.6 \pm 0.3$ s) and the shortest at V3 (mean $T_m = 1.1 \pm 0.2$ s); these short periods reflect the local generation and immature nature of the wave field. The majority of the wave energy was in the range 0.4–0.8 Hz at V1 and V2, and between 0.4 Hz and 1.2 Hz at V3–V5. The 95th percentile of Keulegan–Carpenter numbers at V1 ranged from 10 to 82.

Wave dissipation

During periods of northward waves (D_p within $\pm 20°$ of the transect orientation), wave dissipation generally scaled with wave height (Fig. 5). This quantity (Eq. 2) represents net dissipation that also includes any wave generation from wind. The scaling was most evident at V1–V2 and V2–V3, but there was also considerable scatter, along with periods of negative dissipation, i.e., wave generation. Absolute dissipation values were smaller at V3–V4 and V4–V5 than the other sites, and there was generally wave generation between V4 and V5. Past V3, the small dissipation values suggest waves in quasi-steady state, with production from wind balancing dissipation from vegetation and bottom friction. The diverse dissipation patterns among the sites may be related to changes in bathymetry (Fig. 2), the relative importance of local wind-wave generation to the overall wave field, and any changes in vegetation or seabed characteristics within the transect.

In order to interpret the bulk wave dissipation values, we consider the frequency-variable, normalized wave dissipation $\epsilon_{j,norm}$ (Eq. 3) during the northward and southward wave events. This alleviates the heavy dependence of dissipation on wave height (Fig. 5). Here, we focus on averaged values from four wave bursts (20:30–21:30 on 27 May 2015) during the northward event. The average wind direction was 193°, and the average wave direction at V1 was 203°. Maximum $\epsilon_{j,norm}$ at V1–V2 and V2–V3 was about 0.02 m^{-1} Hz^{-1} and was centered around the peak frequencies of the incident stations (Fig. 6). The peak frequencies at V1 and V2 were both about 0.5 Hz, but rose to about 0.8 Hz at and beyond V3. Between V3 and V4, there was remnant dissipation around 0.5 Hz and wave generation at higher frequencies (greater than about 0.6 Hz), potentially from wind regeneration. At V4–V5, dissipation was less than 0.005 m^{-1} Hz^{-1} and generally was focused between 0.6 Hz and 1 Hz. These patterns result in a reduction of peak period as waves propagate northward. This trend was driven primarily by dissipation at lower frequencies between V1 and V3, and generation at higher frequencies between V3 and V4.

For the southward event, we focus on four wave bursts collected during 13:30–15:00 on 04 June 2015, when the average wind direction was 40° and the average wave direction was 28°. During the southward wave event, between V5 and V4 there was dissipation centered around the peak incoming frequency at V5 ($\sim$ 0.65 Hz) and wave generation around the V4 peak frequency ($\sim$ 0.55 Hz). Between V4 and V3, the peak frequency rose to about 0.8 Hz, with dissipation in excess of 0.01 m^{-1} Hz^{-1} centered around the peak frequency of V4. As waves traveled from V3 to V2, wave dissipation was minor but centered around the V3 peak frequency, and there was considerable wave generation around 0.6 Hz, resulting in a lower peak frequency at V2 as water depth increased (Fig. 2). Wave generation dominated between V2 and V1 and exceeded 0.05 m^{-1} Hz^{-1} as water depth increased along the transect. For these southward waves, as during waves toward to the north, the shifts in peak period resulted from a combination of wave generation and dissipation at different frequencies. For example, the considerable increase in peak period (decrease in peak frequency) between V3 and V1 was due primarily to wave generation at lower frequencies and augmented by wave dissipation at frequencies above about 0.6 Hz. This complex dissipation behavior, especially given the additional wave generation from wind, suggests that a numerical model may be useful in interpreting the data.

Model

We used three parameters to test the agreement between the model and observations: significant wave height H_s, mean period T_m, and net dissipation ϵ. As an integrated quantity, mean period is a more stable parameter than peak period (Wiberg and Sherwood 2008), especially in SWAN model output. Net dissipation for the field data was computed using Eq. 2. This quantity includes all energy sources and sinks and can be negative. For the model output, net dissipation is defined as wave dissipation (including whitecapping, bottom friction, depth-induced breaking, and vegetation) minus wave generation (i.e., wave growth by wind). In

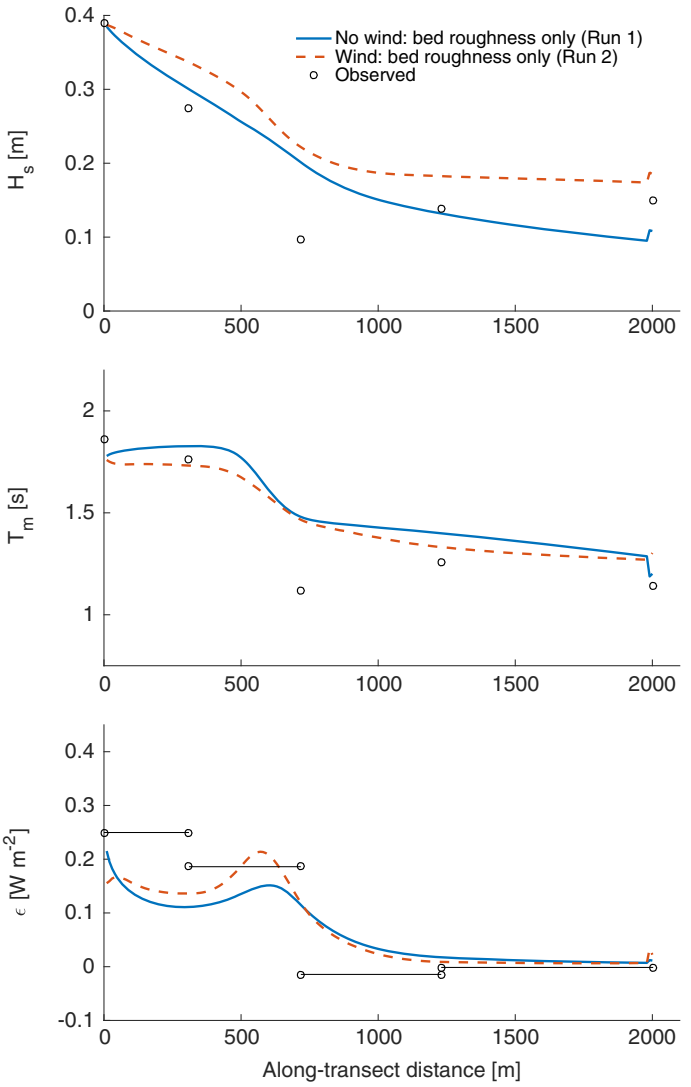

Fig. 7. Observed significant wave height, mean period, and net dissipation (open circles) at 21:00 on 27 May 2015 and model results (curves) for scenarios with and without local wind forcing.

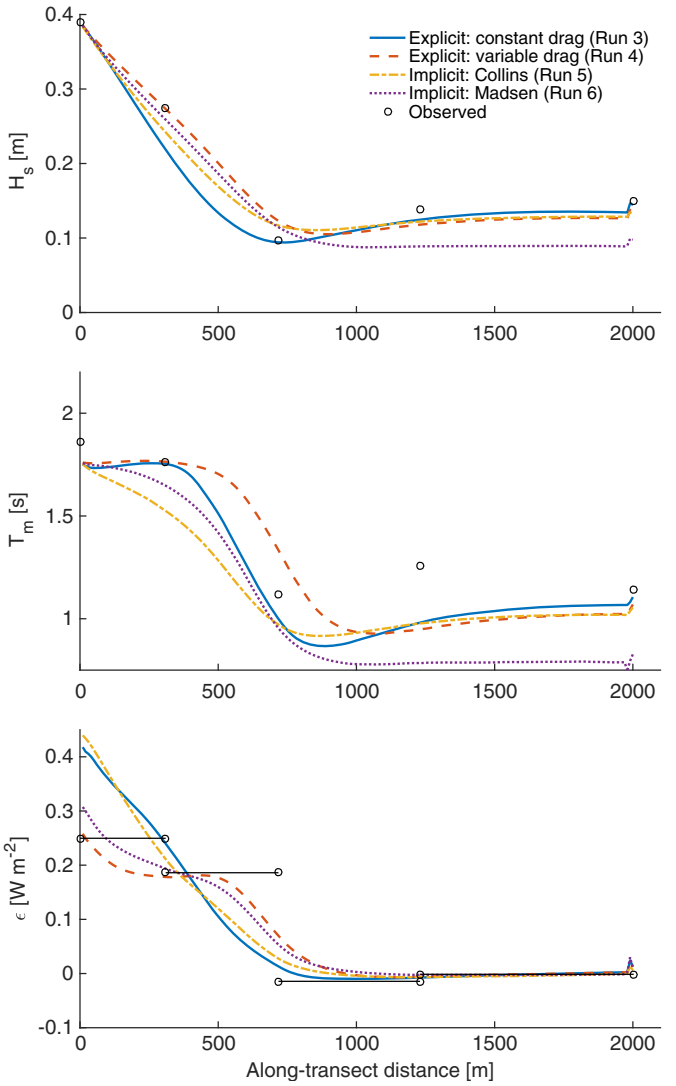

Fig. 8. Observed significant wave height, mean period, and net dissipation (open circles) at 21:00 on 27 May 2015 and model results (curves) for scenarios that explicitly and implicitly represent wave dissipation by vegetation.

addition to these mean parameters, the energy spectra of the different model runs were compared. In this section, six model runs are considered: two that do not attempt to represent vegetation, and four that represent vegetation using different approaches (Table 2).

Wind forcing

Wind forcing is important to observed wave characteristics in the field, and one would expect it to be important to the simulated wave characteristics as well. Runs 1 and 2 test this hypothesis using winds measured at the Assateague wind station. These runs were forced with the observed wave spectra at V1 and realistic bed friction as described earlier. Without wind forcing (Run 1), wave heights reduce monotonically with distance from the model boundary, and the increase in wave heights at V4 and V5 is not observed (Fig. 7). Mean period is over-predicted and, although it decreases near V3, its pattern is distinct from the observed wave period. In contrast to the poor performance of H_s and T_m, the net dissipation patterns and values are generally similar to those observed in the field. The lockstep decrease in wave heights, even with the relatively minimal bed friction imposed by the grain roughness, suggests that wave regeneration by wind is important in this system. When wind forcing is enabled (Run 2), wave heights do not decrease as rapidly as the non-wind case, especially past V3. The relatively constant H_s values downwind of V3 suggest considerable local wave regeneration here, as this region is the

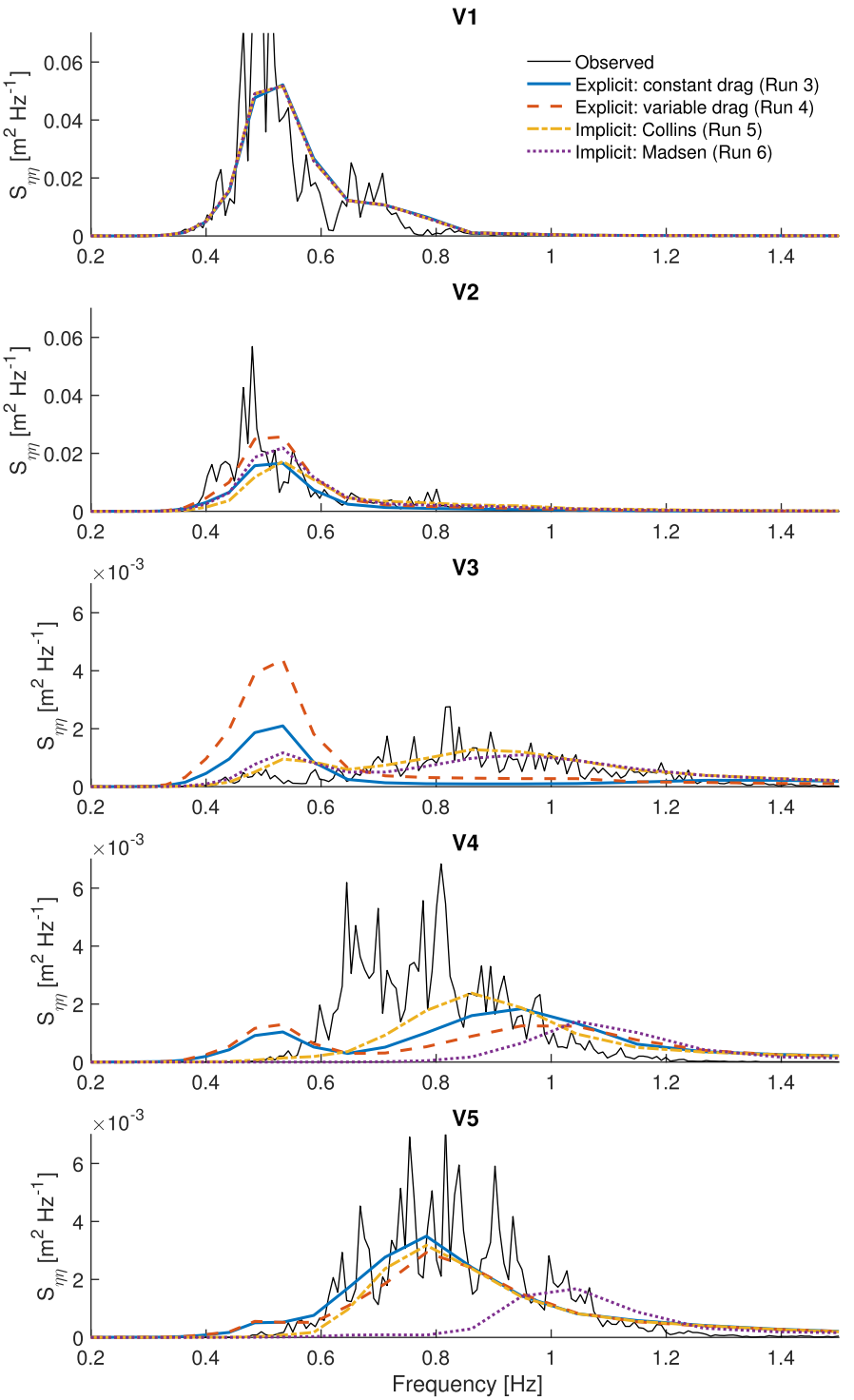

Fig. 9. Observed and modeled wave spectra at 21:00 on 27 May 2015 for runs using explicit vegetation with constant and variable C_D and implicit vegetation using the Collins and Madsen formulations, during the northward wave event. The explicit vegetation approaches over-predict wave energy at low frequencies. Note change in scales between V1, V2 and V3, V4, V5.

shallowest of the domain and experiences wave-height reduction in the absence of wind. The spatial pattern of wave heights remains dissimilar from the observed heights, and H_s in general is over-predicted, suggesting too little bed friction in the model domain. Mean period patterns are similar to the no-wind case and are higher than the observed

values. Wave dissipation is relatively similar between the two cases.

Explicit vegetation

Constant drag coefficient. Because wave heights remain too high with a bed friction coefficient representing the drag imposed by the bed sediment, in this section we consider Run 3, which incorporates greater drag in the form of explicit vegetation. Values for variables in Eq. 9 were chosen as described previously. In this formulation, the single free parameter C_D, allows for tuning of the model to the observed values. The value C_D=0.5 in Eq. 9 gives the best agreement with the field observations, in terms of the significant wave height, mean period, and net dissipation. In this study, C_D was set equal to 0.5 for all runs with constant C_D. The additional drag imposed by the vegetation greatly improves the along-transect patterns and numerical agreement with the observed values (Fig. 8). The model reproduces both the rapid decrease between V1 and V3 and the slight increase through V4 and V5. The patterns in mean period are also reproduced, including the decrease between V2 and V3 and the increase at V4 and V5. Overall, modeled wave periods tended to be underestimates of observed values, which is a relatively common occurrence in SWAN model output (Ris et al. 1999; SWAN Team 2015). Dissipation patterns and magnitudes are similar to those observed in the field data. Values are highest near V1 and steadily decrease until reaching V3, beyond which they remain small. Maximum dissipation is greater than 0.4 W m^{-2} near V1, more than double the mean observed value between V1 and V2 of about 0.2 W m^{-2}.

Variable drag coefficient. In terms of the mean parameters considered here, the variable (KC-dependent) C_D approach (Run 4) performs similarly to that of the constant C_D method (Fig. 8). The pattern and magnitude of wave heights and mean periods are similar, although the decrease in wave period occurs about 100 m farther into the domain than it does for the constant C_D case. Because KC is larger for longer-period waves (such as those found near the start of the transect), the resultant C_D is smaller in the variable-drag formulation. As a result, dissipation at the longer wave periods is delayed, which causes the mean period to remain higher farther into the computational domain. There was, however, better agreement in dissipation with the variable C_D formulation than with the constant C_D approach; the constant drag formulation tended to over-predict dissipation near the beginning of the transect.

Implicit vegetation

Explicit vegetation approaches attempt to represent drag from vegetation via physical characteristics of the plants, along with simplifying assumptions, including that vegetation is treated as a rigid cylinder. As an alternative, the drag imposed by vegetation can be modeled implicitly using bed-friction values that are considerably larger than if they represented only the grain-induced drag. These implicit approaches test the question of whether the additional complexity of physically representing the vegetation characteristics is necessary to faithfully represent the wave field in vegetated environments.

Table 3. Brier Skill Scores, root-mean-square errors, and R^2 values for significant wave height (H_s), mean period (T_m), and net dissipation (ε) at sites V2–V5 for Run 5.

	V2	V3	V4	V5	All
BSS					
H_s	0.718	−0.427	−0.155	−0.308	0.606
T_m	−3.330	−0.611	−7.477	−3.481	0.196
ε	0.641	0.357	0.031	−0.141	0.770
RMSE					
H_s	0.027	0.035	0.036	0.034	0.033
T_m	0.274	0.211	0.229	0.203	0.201
ε	0.040	0.034	0.009	0.006	0.027
R^2					
H_s	0.77	0.61	0.40	0.42	0.80
T_m	0.51	0.66	0.31	0.26	0.84
ε	0.76	0.54	0.08	0.05	0.80

Collins (1972) formulation. This approach reproduced wave heights about as well as the explicit vegetation schemes, with values falling between the constant and variable drag runs. It also captured the mean period patterns, although the decrease in period began earlier and did not drop as low as the constant-drag case (Fig. 8). Dissipation calculated using Collins (1972) was highly similar to the constant C_D explicit vegetation case and faithfully reproduced the observed dissipation.

Modified Madsen et al. (1988) formulation. In general, the modified Madsen et al. (1988) formulation performed about as well as the other approaches (Fig. 8) when k_s=0.03 m, which corresponds to a grain diameter of 12 mm (medium pebble). This method resulted in wave heights similar to the other explicit and implicit vegetation formulations; it underpredicted wave heights by about 0.05 m past V3 but produced similar results at V1 and V2. Wave period agreement was worse, particularly past V3, where the formulation under-predicted wave periods by about 0.4 s compared to the observations and by about 0.2 s compared to the other model approaches. Wave dissipation was similar to the explicit, variable drag approach and was generally in agreement with the observations.

Spectral comparison

So far we have considered only the mean quantities of significant wave height, mean period, and dissipation. Although these values are useful for quickly assessing model performance, inspection of the wave energy spectra may reveal subtleties in model performance that are obscured in

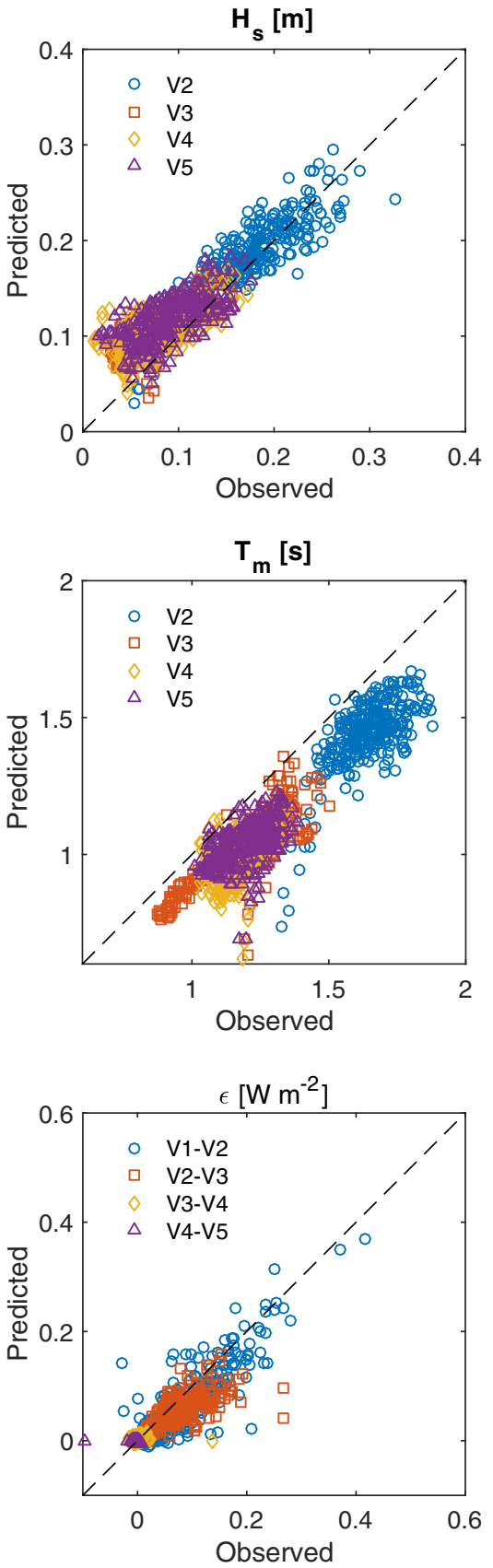

the mean variables. Despite the good agreement in wave height, period, and dissipation when using the explicit vegetation formulations, inconsistencies arise in the modeled energy spectra when compared to the measured spectra (Fig. 9). The explicit vegetation approaches contain too much low-frequency (0.4–0.6 Hz) energy, especially at sites V3–V5. The implicit approaches are in general more faithful in reproducing the observed spectra, although the modified Madsen formulation tends to dissipate too much energy at frequencies below 0.8 Hz, particularly at V4 and V5. The best-performing model was the implicit Collins approach, which generally reproduced the observed spectra at all the sites except for at V3, where it contained too much low-frequency energy.

The excessive low-frequency energy present in the explicit approaches—both constant and variable C_D—may result from the way vegetation dissipation is implemented in SWAN. Contrary to dissipation by bottom friction that dissipates wave energy at different rates depending on frequency, SWAN applies dissipation with a single multiplicative constant across all frequencies (Eq. 9; note the use of mean wavenumber $\tilde{k}$ and mean frequency $\tilde{\sigma}$). Because there is significant low-frequency energy imposed at the boundary, and a single dissipation rate from vegetation is applied across all frequencies, this excess low-frequency energy persists through all of the observation locations. In contrast, the bed-friction formulation of Collins (1972) weights the dissipation toward lower frequencies (Eq. 5; here k and σ can vary, unlike in Eq. 9). The excess of modeled low-frequency energy (or alternatively the dearth of observed low-frequency energy) would seem to be at odds with previous field studies that suggest vegetation preferentially dissipates higher-frequency wave energy. This discrepancy is considered in the Discussion.

Model performance throughout deployment

The approach of Collins (1972) with C_f=0.4 (Run 5) best reproduces the observations during four northward wind events representing 299 half-hourly bursts from the full 2.5 month deployment. The average wind direction of these bursts was 202° with a standard deviation of 12°. The Brier Skill Score (BSS, Brier 1950) was used to evaluate the model, where BSS ranges from 1 (perfect prediction) to $-\infty$. A BSS value of 0 indicates that the model performs as well as the mean of the values would predict each individual value. When considering the full data set at all locations, the BSS shows that the model performs well,

Fig. 10. Performance of Run 5 for 299 half-hourly bursts of northward wind events during the 2.5 month deployment. Top: significant wave height, middle: mean wave period, bottom: net wave dissipation. The dashed line indicates 1 : 1 agreement.

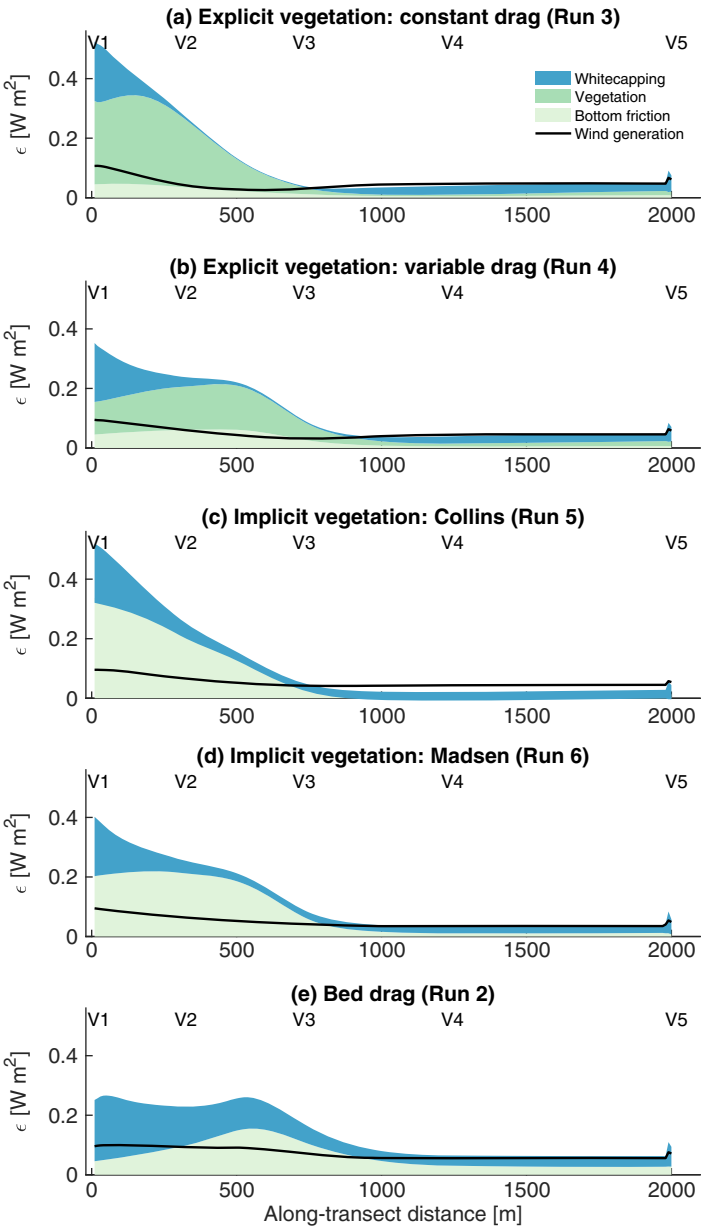

Fig. 11. Modeled wave dissipation from whitecapping, vegetation, and bottom friction, and modeled wave generation from wind, for (**a**) explicit vegetation, constant C_D; (**b**) explicit vegetation, variable C_D; (**c**) implicit vegetation, Collins; (**d**) implicit vegetation, Madsen; and (**e**) bed drag cases. Note that the effect of vegetation is grouped with bottom friction in (**c**) and (**d**), while vegetation is intentionally not represented in (**e**).

especially for wave height and dissipation (Table 3). The score is lower for mean wave period, but this may be expected given the known underprediction of period by SWAN (SWAN Team 2015). Nevertheless, the trends of all three diagnostic variables reproduce the observations (Fig. 10).

To contextualize the model performance further, the root-mean-square error (RMSE) and the coefficient of determination (R^2) were computed for the model predictions. The RMSE was within a few cm for wave heights, approximately 0.25 s for wave period, and 0.04 W m^{-2} for dissipation. These values are within about 10% of the maximum wave height, period, and dissipation, suggesting reasonably good model performance. The model R^2 across all locations was also high—equal to or greater than 0.8—again indicating satisfactory performance of the model.

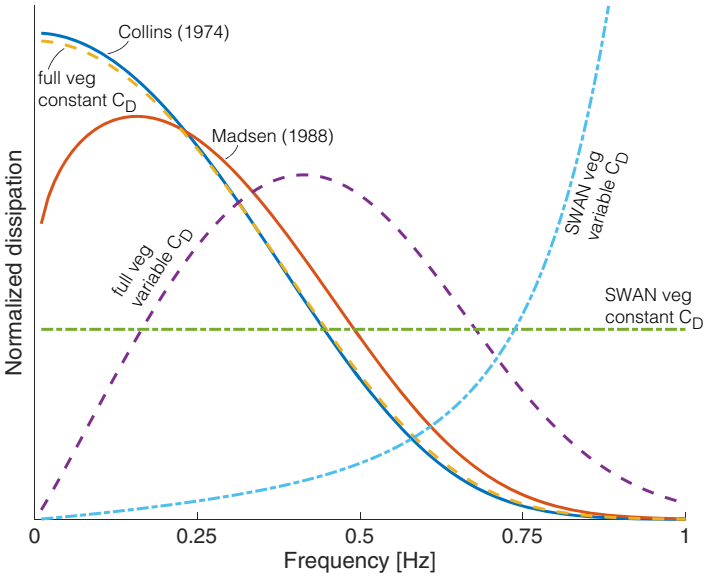

Fig. 12. Normalized dissipation as a function of frequency for several bed-friction and vegetation-drag formulations. The vegetation drag as currently implemented in SWAN is constant across all frequencies, while the bed-friction and variable-C_D implementations preferentially dissipate energy at particular frequencies. The areas under each curve are equivalent.

Discussion

Dissipation sources

Although the explicit and implicit vegetation scenarios all reproduce the observed wave characteristics with acceptable skill, the underlying mechanisms of wave transformation and dissipation in each approach may vary. So far our assumption has been that bed or vegetative friction is the most important source of dissipation; we consider the possibility of other sources, including depth-induced breaking and whitecapping, in this section.

Depth-induced breaking was zero or essentially zero for all scenarios, indicating that, as suggested by the field data (Fig. 4), it is not a significant source of dissipation in this system for the wind and wave conditions considered here. Whitecapping, on the other hand, was a factor in the dissipation distribution (Fig. 11). Whitecapping was most important in the first 100–200 m of the model domain and past 1000 m, although for the explicit and implicit vegetation methods it was the smallest dissipation source compared to the combination of bottom friction and vegetation drag.

When explicitly modeled, vegetation was the most important component of wave dissipation within the first 1000 m of the domain. Its influence was greatest in the constant C_D case; the larger KC in deeper water (i.e., between V1 and V2) resulted in smaller dissipation by vegetation (Eq. 10) in the variable C_D case. Although total dissipation generally decreased between 0 m and 1000 m, the fraction of the total attributable to vegetation increased in that region, as whitecapping became less important. In the implicit vegetation case, the pattern was generally the same as the explicit vegetation case, with the contribution from vegetation wrapped into the bed friction term. The outlier in the scenarios, as expected, was the bed friction-only case. Here, whitecapping was dominant for the first 500 m, and the overall dissipation rate was low, resulting in predicted wave heights that were too high. The dominance of whitecapping within the first 500 m suggests that the imposed wave boundary condition was not sustainable given the model parameters, and bed drag alone was insufficient to reduce the wave heights.

For all runs, wave generation by wind was essential to the dynamics (Fig. 7) but was in general much smaller than dissipation in the first 750–1000 m of the domain. This pattern reflects the net wave dissipation that was present in this region both in the field observations and in all the model scenarios. Past about 1000 m, however, total dissipation was about equal to wave generation, suggesting a quasi-steady-state wave field over the seagrass-colonized shoal.

Influence of vegetation

Prior work has suggested that high-frequency waves are preferentially damped by vegetation. Hansen and Reidenbach (2012) found eelgrass acted as a low-pass filter, reducing high-frequency wave motion and allowing longer periods waves to penetrate the SAV more easily. Bradley and Houser (2009) similarly observed preferential attenuation at higher wave frequencies of 0.75–1 Hz. This behavior potentially arose from phase disagreement between wave velocity and blade velocity: these quantities were in phase for low frequency waves but out of phase at higher frequencies, leading to greater wave attenuation. In the present work, the observed pattern of preferential lower-frequency dissipation is different from these studies. Small-scale vegetation variations could interact with the wave field in complicated ways not

resolvable with the assumption of constant vegetation characteristics, and might contribute to the observed dissipation patterns. The differences may also arise from the variable bathymetry of the study site, as it relates to nonlinear wave–wave interaction, frequency-dependent frictional dissipation, and wave regeneration by wind. Triads can transfer wave energy to higher frequencies when propagating over a bar (Beji and Battjes 1993), a configuration qualitatively similar to the bathymetry in this study (Fig. 2). Triad significance in the model was variable; considerable energy redistribution from triads (up to about 0.2 W m^{-2} at around 600 m) occurred in the bed-only model runs but little (less than 0.01 W m^{-2}) was present in both the implicit and explicit vegetation runs. Energy redistribution from quads was more important, with maximum values of about 0.4 W m^{-2} that rapidly decayed with distance in to the domain. Given that these values are comparable to the total dissipation (Fig. 11), some of the frequency shift seen in the model and observations could arise from these nonlinear processes. When waves typical of those in this work propagate into shallower water, the longer-period waves will experience more dissipation from bottom friction than shorter-period waves (Eq. 5). As a result, the mean period of the wave spectrum will reduce from bathymetry alone, whether vegetation is present or not. It is possible that any preferential patterns in frequency-dependent dissipation by vegetation are masked by these processes which are related to the transect bathymetry. Finally, high-frequency regeneration of waves in the shallow region of the transect (e.g., between V3 and V4; Fig. 6) could influence the overall dissipation pattern and result in the observed preferential low-frequency dissipation.

The different agreement among the model runs also may result from differences in how vegetation is represented. Although the implicit vegetation approach agrees with the observations better than the explicit approach, explicit parameterizations better reflect the underlying physics and may reduce the potential for model over-tuning, if the vegetation characteristics are known. The relatively poor performance of the explicit vegetation module in SWAN can be explained by the fact that SWAN uses mean wavenumber and frequency (Eq. 9) instead of frequency-dependent quantities. As a result, vegetation dissipation (Fig. 12) is not dependent on frequency, in contrast to bottom friction, which is more important at lower frequencies (i.e., longer waves "feel" the bed more than shorter waves). Computing the vegetation dissipation using the full wavenumber and frequency terms reveals a term that follows the trend of bottom friction across frequency space (Fig. 12); in this context we expect the full explicit approach to perform at least as well as the implicit method. Additional mechanisms not accounted for within the current modeling framework include frequency-dependent vortex shedding around vegetation elements, as well as vegetation flexibility. More vortex shedding, and resultant increased dissipation, occur at higher wave frequencies, and may be parameterized by varying the drag coefficient with Keulegan–Carpenter number, as described earlier. These effects result in a band-passed dissipation term that reduces energy the most at moderate wave frequencies (Fig. 12). In the field, this pattern of dissipation may reflect a feedback mechanism between wave conditions and vegetation characteristics (Hansen and Reidenbach 2012). Accounting for SAV flexibility following Luhar and Nepf (2016) does not appreciably change the pattern of wave dissipation with frequency, but the overall dissipation may be reduced because of a decrease (from 30 cm to 7 cm) in the effective blade length.

Applicability to other sites and broader implications

This study was carried out in a unique location, with a specific SAV species present. As such, these results may not be directly applicable to other sites with different biogeomorphic settings. Several northward wind events were used to compute the best-fit C_f value of 0.4 for the Collins (1972) formulation; another approach is to calibrate to a single event and validate with other periods in the deployment. Considering only the late-May event results in a reduced best-fit C_f of 0.3. Applying this smaller value to the full deployment had mixed results, with slightly better BSS agreement for H_s but worse agreement for T_m and ϵ. The results for RMS error and R^2 were also variable, but none of the changes altered the interpretation of the results.

The importance of SAV to local wave transformation becomes more relevant when considering that most operational estuarine numerical models ignore the effects of vegetation on wave dissipation. Our results show that, for this study, SAV reduces wave heights by approximately 25%, based on a comparison of the best-fit Collins model (Fig. 8) and the bed-roughness-only model (Fig. 7). This reduction suggests that the vegetation is essential to the transformation of waves in shallow, open-water environments like Chincoteague Bay. Our results further show that SAV effects on wave dynamics can be successfully modeled using relatively simple bottom-friction formulations, and in fact these formulations can outperform explicit vegetation schemes. In light of this observation, in the type of environment considered here, vegetation may be best parameterized by large bottom friction coefficients.

Regardless of how vegetation is represented, our results contribute to existing work suggesting the considerable importance of vegetation in modifying waves, their resultant wave-induced bed stresses, and associated sediment dynamics. For typical waves considered in this study, wave stress felt at the bed in the presence of vegetation is about 15% less than the stress caused by the larger waves that would be present without vegetation. This reduction in bed stress may promote sediment accumulation, or at least encourage non-erosional conditions. In addition, vegetation likely acts as a geomorphic stabilizer because of its root structure. These two components may act in concert: in Chincoteague Bay, vegetated shoal locations have not migrated appreciably over $\sim$ 25 yr based on inspection of repeat vegetation surveys described in Orth

et al. (2014), suggesting the stabilizing effects of vegetation and wave modification are geomorphically relevant.

This study has demonstrated the importance of SAV in transforming waves in a shallow, open-water environment. This process is inherently local given the rapid response of waves to wind forcing and biogeomorphic feedback. The importance of this localized wave transformation to wave attack at the shoreline, which may be relatively unaffected by remote seagrass meadows, remains to be seen. In any case, the field and model results suggest that the wave characteristics along the transect include a significant contribution from vegetation drag and are not simply due to bed friction alone. Any realistic representation of bed friction based on the grain size greatly underestimates the wave damping observed in the field (Fig. 7).

References

Alves, J. H. G. M., and M. L. Banner. 2003. Performance of a saturation-based dissipation-rate source term in modeling the fetch-limited evolution of wind waves. J. Phys. Oceanogr. **33**: 1274–1298. doi:10.1175/1520-0485(2003)033<1274:POASDS>2.0.CO;2

Bartberger, C. E. 1976. Sediment sources and sedimentation rates, Chincoteague Bay, Maryland and Virginia. J. Sediment. Petrol. **46**: 326–336. doi:10.1306/212F6F50-2B24-11D7-8648000102C1865D

Beji, S., and J. Battjes. 1993. Experimental investigation of wave propagation over a bar. Coast. Eng. **19**: 151–162. doi:10.1016/0378-3839(93)90022-Z

Booij, N. 1983. A note on the accuracy of the mild-slope equation. Coast. Eng. **7**: 191–203. doi:10.1016/0378-3839(83)90017-0

Booij, N., R. C. Ris, and L. H. Holthuijsen. 1999. A third-generation wave model for coastal regions: 1. Model description and validation. J. Geophys. Res. **104**: 7649–7666. doi:10.1029/98JC02622

Bradley, K., and C. Houser. 2009. Relative velocity of seagrass blades: Implications for wave attenuation in low-energy environments. J. Geophys. Res. Earth Surf. **114**: 1–13. doi:10.1029/2007JF000951

Brier, G. W. 1950. Verification of forecasts expressed in terms of probability. Mon. Weather Rev. **78**: 1–3. doi:10.1175/1520-0493(1950)078<0001:VOFEIT>2.0.CO;2

Cavaleri, L., and P. M. Rizzoli. 1981. Wind wave prediction in shallow water: Theory and applications. J. Geophys. Res. **86**: 10961–10973. doi:10.1029/JC086iC11p10961

Collins, J. I. 1972. Prediction of shallow-water spectra. J. Geophys. Res. **77**: 2693–2707. doi:10.1029/JC077i 015p02693

Dalrymple, R. A., J. T. Kirby, and P. A. Hwang. 1984. Wave diffraction due to areas of energy dissipation. J. Waterw. Port Coast. Ocean Eng. **110**: 67–79. doi:10.1061/(ASCE)0733-950X(1984)110:1(67)

Ellis, A. M., M. E. Marot, C. J. Wheaton, J. C. Bernier, and C. G. Smith. 2015. A seasonal comparison of surface sediment characteristics in Chincoteague Bay, Maryland and Virginia, USA. Open-File Report 2015–1219, U.S. Geological Survey. doi:10.3133/ofr20151219.

Folk, R. L. 1954. The distinction between grain size and mineral composition in sedimentary-rock nomenclature. J. Geol. **62**: 344–359. doi:10.1086/626171

Hansen, J. C. R., and M. A. Reidenbach. 2012. Wave and tidally driven flows in eelgrass beds and their effect on sediment suspension. Mar. Ecol. Prog. Ser. **448**: 271–287. doi:10.3354/meps09225

Houser, C., S. Trimble, and B. Morales. 2015. Influence of blade flexibility on the drag coefficient of aquatic vegetation. Estuaries Coasts. **38**: 569–577. doi:10.1007/s12237-014-9840-3

Hsu, S. A., E. A. Meindl, and D. B. Gilhousen. 1994. Determining the power-law wind-profile exponent under near-neutral stability conditions at sea. J. Appl. Meteorol. **33**: 757–765. doi:10.1175/1520-0450(1994)033<0757:DTP LWP>2.0.CO;2

Infantes, E., A. Orfila, G. Simarro, J. Terrados, M. Luhar, and H. Nepf. 2012. Effect of a seagrass (*Posidonia oceanica*) meadow on wave propagation. Mar. Ecol. Prog. Ser. **456**: 63–72. doi:10.3354/meps09754

Johnson, D. 2011. DIWASP, a directional wave spectra toolbox for MATLAB®: User manual. Technical report, Centre for Water Research, University of Western Australia.

Jonsson, I. G. 1966. Wave boundary layers and friction factors. Coast. Eng. Proc. 127–148.

Kobayashi, N., A. W. Raichle, and T. Asano. 1993. Wave attenuation by vegetation. J. Waterw. Port Coast. Ocean Eng. **119**: 30–48. doi:10.1061/(ASCE)0733-950X(1993)119:1(30)

Komen, G. J., S. Hasselmann, and K. Hasselmann. 1984. On the existence of a fully developed wind-sea spectrum. J. Phys. Oceanogr. **14**: 1271–1285. doi:10.1175/1520-0485(1984)014<1271:OTEOAF>2.0.CO;2

Kuik, A. J., G. P. van Vledder, and L. H. Holthuijsen. 1988. A method for the routine analysis of pitch-and-roll buoy wave data. J. Phys. Oceanogr. **18**: 1020–1034. doi:10.1175/1520-0485(1988)018<1020:AMFTRA>2.0.CO;2

Luhar, M., S. Coutu, E. Infantes, S. Fox, and H. Nepf. 2010. Wave-induced velocities inside a model seagrass bed. J. Geophys. Res. Oceans **115**: 1–15. doi:10.1029/2010JC006345

Luhar, M., and H. M. Nepf. 2016. Wave-induced dynamics of flexible blades. J. Fluids Struct. **61**: 20–41. doi:10.1016/j.jfluidstructs.2015.11.007

Madsen, O. S., Y. K. Poon, and H. C. Graber. 1988. Spectral wave attenuation by bottom friction: Theory. Coast. Eng. Proc. **21**: 492–504.

Mendez, F. J., and I. J. Losada. 2004. An empirical model to estimate the propagation of random breaking and nonbreaking waves over vegetation fields. Coast. Eng. **51**: 103–118. doi:10.1016/j.coastaleng.2003.11.003

Nepf, H. M. 2012. Flow and transport in regions with aquatic vegetation. Annu. Rev. Fluid Mech. **44**: 123–142. doi:10.1146/annurev-fluid-120710-101048

Nielsen, P. 1992. Coastal bottom boundary layers and sediment transport. World Scientific.

Orth, R. J., D. J. Wilcox, J. R. Whiting, L. Nagey, A. K. Kenne, and E. R. Smith. 2014. 2013 Distribution of submerged aquatic vegetation in Chesapeake Bay and coastal bays. Technical report, Virginia Institute of Marine Science.

Paul, M., and C. L. Amos. 2011. Spatial and seasonal variation in wave attenuation over *Zostera noltii*. J. Geophys. Res. Oceans **116**: 1–16. doi:10.1029/2010JC006797

Ris, R. C., L. H. Holthuijsen, and N. Booij. 1999. A third-generation wave model for coastal regions: Verification. J. Geophys. Res. **104**: 7667–7681. doi:10.1029/1998JC9 00123

Sánchez-González, J. F., V. Sánchez-Rojas, and C. D. Memos. 2011. Wave attenuation due to *Posidonia oceanica* meadows. J. Hydraul. Res. **49**: 503–514. doi:10.1080/00221686.2011.552464

Soulsby, R. 1997. Dynamics of marine sands. Telford.

Stevens, A. W., and J. R. Lacy. 2012. The influence of wave energy and sediment transport on seagrass distribution. Estuaries Coast. **35**: 92–108. doi:10.1007/s12237-011-9435-1

Suzuki, T., M. Zijlema, B. Burger, M. C. Meijer, and S. Narayan. 2012. Wave dissipation by vegetation with layer schematization in SWAN. Coast. Eng. **59**: 64–71. doi:10.1016/j. coastaleng.2011.07.006

SWAN Team. 2015. SWAN scientific and technical documentation. Technical report, Delft University of Technology.

Swart, D. H. 1974. Offshore sediment transport and equilibrium beach profiles. Technical report, Delft Hydraulics Laboratory, Delft.

Thornton, E. B., and R. T. Guza. 1983. Transformation of wave height distribution. J. Geophys. Res. **88**: 5925. doi:10.1029/JC088iC10p05925

van Katwijk, M., A. Bos, D. Hermus, and W. Suykerbuyk. 2010. Sediment modification by seagrass beds: Muddification and sandification induced by plant cover and environmental conditions. Estuar. Coast. Shelf Sci. **89**: 175–181. doi:10.1016/j.ecss.2010.06.008

WAMDI Group. 1988. The WAM model—a third generation ocean wave prediction model. J. Phys. Oceanogr. **18**: 1775–1810. doi:10.1175/1520-0485(1988)018<1775:TWMTGO>2.0.CO;2

Wiberg, P. L., and C. R. Sherwood. 2008. Calculating wave-generated bottom orbital velocities from surface-wave parameters. Comput. Geosci. **34**: 1243–1262. doi:10.1016/j.cageo.2008.02.010

Acknowledgments

We thank Tomohiro Suzuki for helpful conversations regarding the vegetation implementation in SWAN. Jeremy Testa performed the vegetation surveys, Steve Suttles was instrumental to the success of the fieldwork, and Brian Andrews produced the Chincoteague bathymetric grid. The constructive comments of Curt Storlazzi, two anonymous reviewers, and the associate editor improved the manuscript. Data analyzed in this study are available at http://dx.doi.org/10.5066/F7DF6PBV. This study was part of the Estuarine Physical Response to Storms project (GS2-2D), supported by the Department of the Interior Hurricane Sandy Recovery program. Any use of trade, firm, or product names is for descriptive purposes only and does not imply endorsement by the U.S. Government.

Conflict of Interest

None declared.

Submitted 01 April 2016
Revised 27 July 2016
Accepted 21 September 2016

Associate editor: Josef Ackerman